arXiv:1611.05282v1 [cond-mat.soft] 15 Nov 2016

Non-linear rheology in a model biological tissue

D. A. Matoz-Fernandez,[1,*] Elisabeth Agoritsas,[1,2,†] Jean-Louis Barrat,[1] Eric Bertin,[1] and Kirsten Martens[1]

[1] *Université Grenoble Alpes & CNRS, LIPHY, F-38000 Grenoble, France*
[2] *Laboratoire de Physique Théorique, Ecole Normale Supérieure, F-75005 Paris, France*

Mechanical signaling plays a key role in biological processes like embryo development and cancer growth. One prominent way to probe mechanical properties of tissues is to study their response to externally applied forces. Using a particle-based model featuring random apoptosis and environment-dependent division rates, we evidence a crossover from linear flow to a shear-thinning regime with increasing shear rate. To rationalize this non-linear flow we derive a theoretical mean-field scenario that accounts for the interplay of mechanical and active noise in local stresses. These noises are respectively generated by the elastic response of the cell matrix to cell rearrangements and by the internal activity.

Mechanical stimuli on single cells [1] and cell assemblies [2] play an important role in biology, for example in the mechanics of biofilms [3] as well as for medical issues [4, 5]. The most prominent example where mechanical sensing has been shown to be of vital importance is without doubt in the context of cancer growth [6–8].

Driven by advances in experimental cell tracking techniques [9, 10], this topic has gained a lot of importance in the recent years. The mechanical response of cell aggregates under deformation has been shown to exhibit elastic, elasto-plastic and viscous flow behavior depending on the forces applied and the time scale of observation considered [10–12]. Recently there have been many efforts to understand the origin of these different mechanical regimes. It has been shown that both self-propulsion [13–16] and cell-division and apoptosis [17–19] are processes able to fluidize a confluent cell assembly, that appears to be arrested in a glassy configuration otherwise.

In this letter we go beyond the study of the specific fluidization mechanism and the corresponding linear flow regime [18]. We investigate the flow properties of a confluent tissue under shear using a particle-based model that incorporates activity in the form of cell division and apoptosis [19]. We find that the internal activity gives rise to a fluidization of the tissues at shear rates smaller than a time scale set by the apoptosis rate, followed by a shear-thinning regime, well described by a Herschel-Bulkley flow curve at higher shear rates.

In analogy to the flow of soft matter, such as emulsions or foams, we propose a statistical description to derive an analytical prediction for the complex flow curve in confluent tissues. At the core of this description is an elasto-plastic picture: the inactive cell assembly responds elastically to external forcing like a solid up to a threshold above which it is able to locally yield through cell-cell rearrangements leading to plastic flow as shown in the stress-strain curve in the bottom panel of Fig. 1. The local rearrangements (T1 events, see sketch in Fig. 1) lead to a long-range elastic response of the surrounding medium that will create a mechanical noise [20]. We argue that the elastic perturbation created through the internal activity, for example via cell division and apoptosis

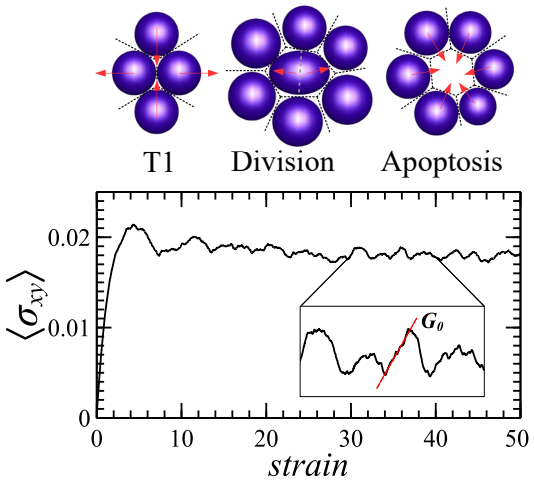

FIG. 1. (*Top*) Microscopic events in a system with cell division and apoptosis under shear. From left to right, T1 event (passive rearrangement), cell division and apoptosis (active rearrangements). (*Bottom*) Typical macroscopic stress-strain curve, the average slope of the increasing elastic parts on the curve corresponds to the elastic modulus G_0.

(sketch in Fig. 1), creates an additional active noise. The interplay of these different mechanisms leads to an interesting non-trivial flow behavior. We rationalize these findings using a mean-field description that extends the Hébraud-Lequeux model [1] of athermal yield stress fluids.

In spite of the inherent complexity of tissue mechanics, many interesting collective phenomena at tissue level can be described using simple models in which cell-cell interactions are treated as soft interactions between particles [5, 23]. In this spirit, we model a tissue as a collection of N soft spherical particles with radii b_i uniformly distributed in a range of 0.85 to 1.15. Moreover, in order to mimic the real behavior of cells in epithelial sheets we consider adhesion and excluded volume as a combination

of attractive and repulsive forces [19, 24],

$$\mathbf{F}_{ij} = \begin{cases} -kb_{ij}\left(1 - \frac{r_{ij}}{b_{ij}}\right)\hat{\mathbf{r}}_{ij} & \text{if } 0 \le \frac{r_{ij}}{b_{ij}} \le \epsilon + 1 \\ kb_{ij}\left(2\epsilon + 1 - \frac{r_{ij}}{b_{ij}}\right)\hat{\mathbf{r}}_{ij} & \text{if } \epsilon < \frac{r_{ij}}{b_{ij}} - 1 \le 2\epsilon, \end{cases} \quad (1)$$

where k is the stiffness constant, $b_{ij} = b_i + b_j$ is the sum of the particles radii and ϵ is the ratio of the maximal attractive and maximal repulsive forces. The cell centroids $\mathbf{r}_i(t)$ follow an overdamped dynamics, $\partial_t \mathbf{r}_i(t) = \mu \mathbf{F}_i$, where μ is the mobility coefficient [6]. In addition, activity is introduced via apoptosis and cell-division rates. Apoptosis (as well as possibly other cell death mechanisms) is included by removing cells randomly at constant rate a. On the other hand, as in real epithelial tissues, the contact inhibition process [26] is modeled via a density-dependent division rate $d_i = d_0(1 - z_i/z_{\max})$, with d_0 the division rate amplitude, z_i the number of contact neighbors of particle i, and $z_{\max}$ the maximum number of contact neighbors allowed. After any division, the new daughter cell is placed on top of the mother cell. In order to prevent any numerical instability, the total force exerted by the mother and daughter cells on the surrounding cells is kept continuous, by applying only a half force immediately after cell division, and then progressively increasing the applied force to reach again a nominal force applied on each cell [19].

We carried out 2D simulations of the model with fixed values of $\mu = k = 1$, $z_{\max} = 6$, and $\epsilon = 0.05$ using a C++ GPU-parallel Molecular Dynamics code [27]. We take as control parameter the apoptosis rate a. As varying a at fixed maximal division rate d_0 would lead to large variations in packing fraction. Here, we rather fix d_0 through the relation $a/d_0 = 0.1$, leading to limited changes of the packing fraction.

After a steady state has been reached in the absence of shear, with the average division rate balancing the apoptosis rate, we impose shear by deforming the box at a constant shear rate $\dot{\gamma}$. We then measure the macroscopic shear stress $\sigma_{xy}(t)$, as illustrated in Fig. 1, and we consider that the stationary state under shear is reached after 100% strain.

We have established that the homeostatic properties of the system do not strongly depend on a [27]. For low enough shear rate $\dot{\gamma}$ and apoptosis rate a, the packing fraction is constant [Fig. 2(b)]. A careful analysis of the packing fraction Φ as a function of a and $\dot{\gamma}$ [Fig. 2(b)] however reveals two different regimes in which the packing fraction deviates from this constant value. First, considering a fixed low shear rate (typically $\dot{\gamma} < 10^{-3}$), the packing fraction Φ increases with activity if $a \gtrsim 10^{-3}$. This is understood as an interplay between the division rate d_0 (equal to $0.1a$) and the mechanical relaxation rate μk in the soft repulsive potential [19]. As long as the elastic relaxation time $\tau_{\rm el} = (\mu k)^{-1}$ remains small with respect to the typical time $\tau_{\rm a} = (d_0)^{-1}$ between two

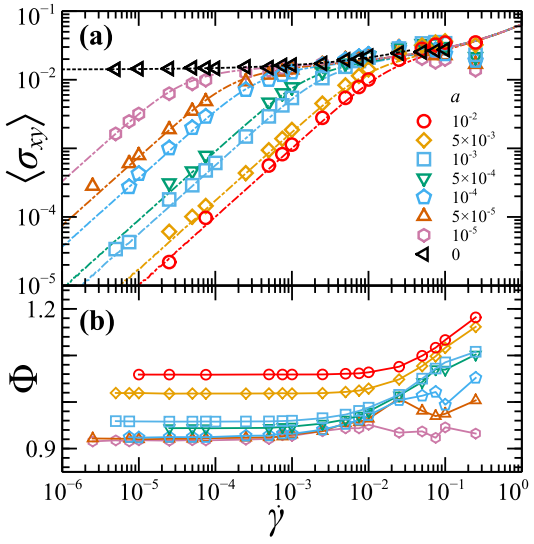

FIG. 2. *Flow curves for passive and active systems* – (a) Steady-state average shear stress $\langle\sigma_{xy}\rangle$ *versus* the applied external shear rate $\dot{\gamma}$ for different apoptosis rates a. The symbols indicated the microscopic simulations results for different apoptosis rates as indicated in the figure. The dashed line corresponds to a Herschel-Bulkley fit of the passive system with packing fraction $\Phi \approx 0.94$. The dashed-dotted lines are the mean-field model fits with fitting parameter D_0. (b) Shear-rate dependence of the corresponding packing fraction Φ for the same values of the apoptosis rates.

divisions involving the same cell, the elastic relaxation processes remain independent and the packing fraction remains constant. When, in constrast, $\tau_{\rm a} \ll \tau_{\rm el}$, multiple divisions occur during the elastic relaxation, and the resulting packing fraction depends on the activity a. The second regime is related to the effect of a strong enough shear rate, typically $\dot{\gamma} > 10^{-3}$. In this case, we observe that a fast and large deformation of the box produces a rapid decrease of the number of contact neighbors followed by an increase of the division rate, eventually leading to a steady state with a higher packing fraction.

The corresponding flow curves, i.e. the steady-state macroscopic stress $\langle\sigma_{xy}\rangle$ as a function of $\dot{\gamma}$, are shown in Fig. 2(a) for different values of the apoptosis rate. In the absence of activity ($a = 0$) the system exhibits a nonlinear rheology as observed in foams; it is well known that this type of dynamics is then characterized at low shear rates by a Herschel-Bulkley flow curve $\langle\sigma_{xy}\rangle = \sigma_y^{(d)} + A_{\rm HB}\dot{\gamma}^n$. In other words, in the limit of zero shear rate, the macroscopic stress takes a finite value, known as the dynamical yield stress $\sigma_y^{(d)}$, and then increases with the shear rate following a power-law behavior [28]. In our case, we obtain $\sigma_y^{(d)} = 0.014$, $A_{\rm HB} = 0.065$ and $n \approx 0.5$ for $\dot{\gamma} \le 0.025$ (see dashed curve), this exponent being consistent with those observed in foams and in recent molecular dynamics simu-

lations [20]. On the other hand, a finite activity $a > 0$ prevents the system from having a finite yield stress $\sigma_y^{(d)}$, leading to a linear behavior at low shear rates, with a viscosity that decreases when a increases. Here the new feature is the crossover, at a shear rate $\dot{\gamma}^*$ controlled by the activity, from a Newtonian to a Herschel-Bulkley behavior. Defining the crossover as the intersection between the linear regime and the plateau, we have plotted $\dot{\gamma}^*(a)$ in Fig. 3(b), obtaining an almost linear dependence $\dot{\gamma}^* \sim a^{0.82}$. We emphasize that, at least for small enough activity ($a \lesssim 10^{-4}$), the crossover from activity-driven fluidization to a yield-stress (plateau) behavior occurs at a constant packing fraction. On the contrary, the stress increase at large shear rate $\dot{\gamma}$ results from both standard elasto-plastic effects and the increase of the packing fraction.

The crossover from linear to non-linear flow behaviors of the sheared active system can be captured via a minimal mean-field description that focuses on the dynamics of the local shear stress. For this purpose, we use an athermal-local-yield-stress model [2, 3], which generalizes the original Hébraud-Lequeux model [1]. These models usually do not take into account any active contribution to the local stress fluctuations. As shown in Fig. 2(a), this active contribution is however a key ingredient for fluidizing the system and thus introduced explicitly thereafter. In a simplified mean-field picture, the dynamics of the local stress can be modeled by a modified Langevin dynamics, $\partial_t \sigma(t) = G_0 \dot{\gamma} + \xi_{\rm mec}(t)$ with G_0 the average local elastic modulus, $\dot{\gamma}$ the external constant shear rate, and $\xi_{\rm mec}(t)$ the mechanical noise. In addition, once $\sigma(t)$ exceeds a typical threshold σ_c, a local plastic event randomly occurs at a fixed rate $1/\tau$, which would in turn fully relax the local stress and thus reset $\sigma(t)$ to 0. Here, $\xi_{\rm mec}(t)$ is modeled by a Gaussian noise with zero mean. Furthermore, at the time scale we consider, we can neglect its time correlation, i.e. $\langle \xi_{\rm mec}(t)\xi_{\rm mec}(t')\rangle = 2D(t)\delta(t-t')$, where the brackets corresponds to average over time, and $D(t)$ is the stress diffusion coefficient. At low shear rate, a natural way to introduce activity is to distinguish two contributions to the noise, i.e. $\xi_{\rm mec}(t) = \xi_{\rm pl}(t) + \xi_{\rm act}(t)$. The noise $\xi_{\rm pl}(t)$ accounts for the plastic events triggered by the external driving throughout the system, and has a time-dependent diffusion coefficient $D_{\rm pl}(t)$. The noise $\xi_{\rm act}(t)$ corresponds to the stress fluctuations produced by activity (cell division and apoptosis), and has a time-independent diffusion coefficient D_0. We assume that these two competing noises are statistically independent. Hence, the stress diffusion coefficient has two additive contributions, $D(t) = D_{\rm pl}(t) + D_0$. Following the standard Hébraud-Lequeux model [1], the diffusion coefficient $D_{\rm pl}(t)$ modeling the effect of plastic events is self-consistently determined as $D_{\rm pl}(t) = \alpha\,\Gamma(t)$, where $\Gamma(t)$ is the global plastic activity and α is a coupling parameter related to the elastic stress propagator [2, 27, 31]. Here, we emphasize that

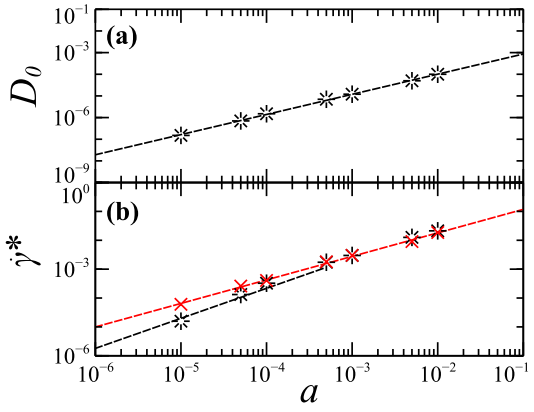

FIG. 3. (a) Fitted value of the diffusion coefficient D_0 of the active noise as a function of the apoptosis rate a from the mean-field fit on the simulation data. The dashed line is a power-law fit with an exponent 0.94. (b) Activity-dependent crossover shear rate $\dot{\gamma}^*(a)$ measured from the flow curves (see text for details). Crosses are determined values from the pure simulation data, whereas stars come from the mean-field fit of the simulations.

the new key ingredient is the diffusion coefficient $D_0 > 0$ stemming from activity. The macroscopic stress $\langle \sigma_{xy}\rangle$ can be obtained from the probability distribution of local stress σ. The evolution equation of this distribution is,

$$\begin{aligned}\partial_t \mathcal{P}(\sigma,t) = &- G_0\dot{\gamma}\,\partial_\sigma \mathcal{P} + (\alpha\,\Gamma(t) + D_0)\;\partial_\sigma^2 \mathcal{P} \\ &- \frac{1}{\tau}\theta(|\sigma| - \sigma_c)\,\mathcal{P} + \Gamma(t)\,\delta(\sigma)\end{aligned} \tag{2}$$

where $\Gamma(t) = \frac{1}{\tau}\int_{|\sigma|>\sigma_c} d\sigma\,\mathcal{P}(\sigma,t)$ is the average number of sites that yield per unit time; $\Gamma(t)$ is proportional to the number of sites that have reached the threshold (i.e. $|\sigma_i| > \sigma_c$) divided by the "lifetime" τ [1, 2]. The stress on these sites is reset to zero after the yield event.

In the steady state at constant shear rate, and in the absence of activity ($D_0 = 0$), it is well known that this mean-field model predicts the existence of a Herschel-Bulkley regime with an exponent $n = 1/2$ at low $\dot{\gamma}$ and for $\alpha < \sigma_c^2/2$ [1–3].

In the presence of activity ($D_0 > 0$), the present mean-field model reproduces the fluidization process leading to a linear behavior (i.e. Newtonian regime) and, quite importantly, recovers a non-linear flow curve beyond a crossover shear rate $\dot{\gamma}^*$,

$$\langle \sigma_{xy}\rangle \approx \begin{cases} \eta\,\dot{\gamma} & \text{if } \dot{\gamma} < \dot{\gamma}^* \\ \sigma_y + A_{\rm HB}\,\dot{\gamma}^{1/2} & \text{if } \dot{\gamma} > \dot{\gamma}^* \end{cases} \tag{3}$$

as observed in Fig. 2. Analytical calculations show that $\dot{\gamma}^* \sim D_0$ for $D_0 \to 0$. The explicit expressions for $\{\eta, \sigma_y, A_{\rm HB}, \dot{\gamma}^*\}$ can be computed as a function of the model parameters $\{G_0, \tau, \sigma_c, \alpha, D_0\}$, using the methods described in Ref. [2] —Supplementary Material [27].

To compare the mean-field model with the numerical data of the particle-based model, we have to fit the values of the model parameters $\{G_0, \tau, \sigma_c, \alpha, D_0\}$. We used the following fitting procedure. First, the elastic modulus G_0 is estimated independently from the initial elastic response in the stress-strain curve (see Fig. 1) yielding $G_0 \approx 0.25$. Secondly, the parameters $\{\tau, \sigma_c, \alpha\}$ are fitted on the flow curve obtained in the absence of activity ($a = 0$, $\Phi \approx 0.94$), in turn yielding $\tau = 0.12$, $\sigma_c = 0.15$, and $\alpha = 0.45\sigma_c^2$. Having fixed the four parameters $\{G_0, \tau, \sigma_c, \alpha\}$, we then fit the different flow curves obtained in the active case ($a > 0$) with D_0 as the only free parameter. The procedure eventually yields the fitted value $D_0(a)$, which is plotted in Fig. 3(a). As expected, the fitted value of σ_c is larger than σ_y, see Eq. 3 , and that the coupling α is smaller than $\sigma_c^2/2$ as required to observe a Herschel-Bulkley behavior. We further observe that the obtained value of α/σ_c^2 is larger than for the Lennard-Jones systems [20]; we attribute this larger value to the presence of a softer potential. More importantly, the stress diffusion coefficient $D_0(a)$ fitted from the mean-field prediction is plotted in Fig. 4(a), and scales fairly linearly with a. This can be understood as follows. At low a, apoptosis events are rare and independent, so we can safely assume that the typical redistributed stress $\Delta\sigma$ after such events will depend only on the packing fraction but not on the activity. Moreover, at low shear rates the only relevant timescale is set by the apoptosis rate. Thus we can estimate the stress diffusion coefficient D_0 by simple scaling argument as $D_0 \sim \Delta\sigma^2 a$. Furthermore, the mean-field picture predicts a crossover $\dot{\gamma}^*$ linear with D_0, and hence we expect $\dot{\gamma}^* \sim a$, consistently with the flow curve crossover shown in Fig. 3(b).

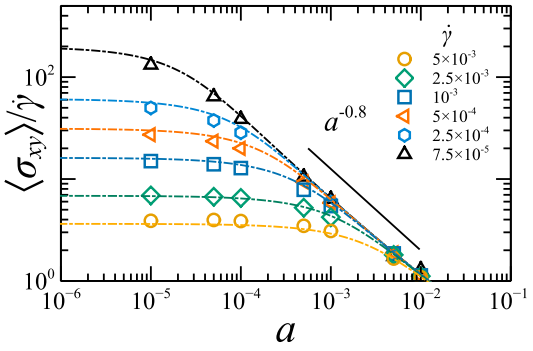

FIG. 4. Viscosity $\eta = \langle\sigma_{xy}\rangle/\dot{\gamma}$ as a function of the apoptosis rate a for different small values of the shear rate (symbols for the numerical data and dash-dotted lines for mean-field prediction).

To provide further insights on the behavior of our model, we show in Fig. 4 the activity-dependent viscosity $\eta = \langle\sigma_{xy}\rangle/\dot{\gamma}$ for different fixed, low values of the shear rate. We observe that the viscosity decreases when activity is enhanced beyond a (strain-rate-dependent) threshold value, i.e. fluidizing the system as previously reported in [17]. However, the Maxwell picture proposed in [17] cannot capture the crossover to the non-linear rheology that we observe in Fig. 2(a). This is due to the fact that the plateau in the viscosity observed at low activity [see Fig. 4] does not correspond to a Newtonian regime (in which the shear stress varies linearly with $\dot{\gamma}$), but rather to a yield stress fluid behavior. This is clearly seen from the fact that the plateau value of the viscosity strongly depends on the strain rate $\dot{\gamma}$, a property that cannot be accounted for by a simple Maxwell model. The data presented in Fig. 4 can be understood as follows. At low enough activity, plasticity is dominant and the shear stress remains independent of activity. For a fixed shear rate, the viscosity $\eta = \langle\sigma_{xy}\rangle/\dot{\gamma}$ is thus independent of activity, yielding the plateau in Fig. 4. At higher activity, the active contribution to the mechanical noise instead becomes dominant, thus decreasing the viscosity. In this regime, the mean-field model predicts $\eta \sim 1/D_0$ (see Supplementary Material [27]), in good agreement with Fig. 4 (dashed-dot lines), taking into account $D_0 \sim a$. Note here again the good agreement between the mean-field model and the numerical simulations.

In conclusion, we proposed in this letter a generic scenario to understand the crossover from linear to non-linear rheology in flowing active tissues, based on stress fluctuations mediated by long-range elastic interactions. The mean-field picture presented here allows us to introduce explicitly the interplay of the two relevant timescales in these systems, one imposed by the external shear and another by the internal processes of the biological tissue in form of cell division and apoptosis. This scenario is able to rationalize well the numerical findings of our particle-based model for the active confluent tissue under shear, as can be seen from the flow curves and the activity-dependent viscosity.

It has been shown that our mean-field predictions are qualitatively robust to the addition of disorder [2], partial relaxation of stress or effective shear-rate dependence of the elastic modulus or relaxation time [3], assessing furthermore the generality of our scenario. Moreover, the introduction of additional relaxation mechanisms like cell-shape fluctuations, self propulsion, external vibrations and other sources of mechanical noise, can be easily implemented in our mean-field description via assumptions on the distribution of the active part of the noise. However, to allow for a more refined description of the dynamics aiming for a quantitative agreement, it would be interesting to investigate in more details the long-range elastic effects of cell division and apoptosis events. A strong point of our approach is that it can be easily generalized to describe the rheological response of other systems that include an additional shear-rate independent noise, such as vibrated grains [4, 32, 33, 35], active colloidal suspensions [36] or coarsening foams [37, 38].

Acknowledgements. J.-L. B., D. A. M.-F. and E. A. acknowledge financial support from ERC grant ADG20110209; E. A. was also supported by the Swiss National Science Foundation grant No P2GEP2-15586. J.-L. B., D. A. M.-F. and K. M. thanks the NVIDIA Corporation for the hardware grant through the Academic Partnership Program. Further we would like to thank Silke Henkes and Rastko Sknepnek for valuable discussions on the particle model description during this work. D. A. M.-F. and E. A. and contributed equally to this work.

* daniel-alejandro.matoz-fernandez@univ-grenoble-alpes.fr
† elisabeth.agoritsas@lpt.ens.fr

[1] E. Moeendarbary and A. R. Harris, Wiley Interdisciplinary Reviews: Systems Biology and Medicine **6**, 371 (2014).
[2] T. Lecuit and P.-F. Lenne, Nature Reviews. Molecular Cell Biology **8**, 633 (2007).
[3] N. Billings, A. Birjiniuk, T. S. Samad, P. S. Doyle, and K. Ribbeck, Reports on Progress in Physics **78**, 036601 (2015).
[4] C. R. Jacobs, H. Huang, and R. Y. Kwon, *Introduction to Cell Mechanics and Mechanobiology* (Garland Science, 2013).
[5] A. van den Berg and L. Segerink, eds., *Microfluidics for Medical Applications*, RSC Nanoscience & Nanotechnology (The Royal Society of Chemistry, 2015) pp. P001–303.
[6] M. J. Paszek, N. Zahir, K. R. Johnson, J. N. Lakins, G. I. Rozenberg, A. Gefen, C. A. Reinhart-King, S. S. Margulies, M. Dembo, D. Boettiger, *et al.*, Cancer Cell **8**, 241 (2005).
[7] M. Delarue, F. Montel, D. Vignjevic, J. Prost, J.-F. Joanny, and G. Cappello, Biophysical Journal **107**, 1821 (2014).
[8] A. Nagelkerke, J. Bussink, A. E. Rowan, and P. N. Span, Seminars in Cancer Biology **35**, 62 (2015), complexity in Cancer Biology.
[9] X. Trepat, M. R. Wasserman, T. E. Angelini, E. Millet, D. A. Weitz, J. P. Butler, and J. J. Fredberg, Nature Physics **5**, 426 (2009).
[10] T. E. Angelini, E. Hannezo, X. Trepat, M. Marquez, J. J. Fredberg, and D. A. Weitz, Proceedings of the National Academy of Sciences **108**, 4714 (2011).
[11] P. Marmottant, A. Mgharbel, J. Kaefer, B. Audren, J.-P. Rieu, J.-C. Vial, B. van der Sanden, A. F. M. Marée, F. Graner, and H. Delanoe-Ayari, Proceedings of the National Academy of Sciences **106**, 17271 (2009).
[12] S. Heermann, L. Schütz, S. Lemke, K. Krieglstein, and J. Wittbrodt, Elife **4**, e05216 (2015).
[13] L. Berthier, Physical Review Letters **112**, 220602 (2014).
[14] R. Mandal, P. J. Bhuyan, M. Rao, and C. Dasgupta, Soft Matter **12**, 6268 (2016).
[15] D. Bi, X. Yang, M. C. Marchetti, and M. L. Manning, Physical Review X **6**, 021011 (2016).
[16] G. Szamel, E. Flenner, and L. Berthier, Physical Review E **91**, 062304 (2015).
[17] J. Ranft, M. Basan, J. Elgeti, J.-F. Joanny, J. Prost, and F. Jülicher, Proceedings of the National Academy of Sciences **107**, 20863 (2010).
[18] M. Basan, J. Prost, J.-F. Joanny, and J. Elgeti, Physical Biology **8**, 026014 (2011).
[19] D. Matoz Fernandez, K. Martens, R. Sknepnek, J. L. Barrat, and S. Henkes, "Fluidization of tissues due to cell division and apoptosis," arXiv:1610.09340 [cond-mat.soft] (2016).
[20] F. Puosi, J. Olivier, and K. Martens, Soft Matter **11**, 7639 (2015).
[1] P. Hébraud and F. Lequeux, Physical Review Letters **81**, 2934 (1998).
[5] D. Drasdo, S. Hoehme, and M. Block, Journal of Statistical Physics **128**, 287 (2007), 34249873259.
[23] J. Zimmermann, B. A. Camley, W.-J. Rappel, and H. Levine, Proceedings of the National Academy of Sciences **113**, 2660 (2016).
[24] B. Szabó, G. J. Szöllösi, B. Gönci, Z. Jurányi, D. Selmeczi, and T. Vicsek, Physical Review E **74**, 061908 (2006).
[6] S. Henkes, Y. Fily, and M. C. Marchetti, Physical Review E **84**, 84 (2011), 1107.4072.
[26] A. Puliafito, L. Hufnagel, P. Neveu, S. Streichan, A. Sigal, D. K. Fygenson, and B. I. Shraiman, Proceedings of the National Academy of Sciences **109**, 739 (2012).
[27] See Supplemental Material.
[28] W. H. Herschel and R. Bulkley, Kolloid-Zeitschrift **39**, 291 (1926).
[2] E. Agoritsas, E. Bertin, K. Martens, and J.-L. Barrat, European Physical Journal E: Soft Matter **38**, 71 (2015).
[3] E. Agoritsas and K. Martens, "Nontrivial rheological exponents in sheared yield stress fluids," arXiv:1602.03484 [cond-mat.soft] (2016).
[31] L. Bocquet, A. Colin, and A. Ajdari, Physical Review Letters **103**, 036001 (2009).
[32] G. D'anna, P. Mayor, A. Barrat, V. Loreto, and F. Nori, Nature **424**, 909 (2003).
[33] K. J. Ford, J. F. Gilchrist, and H. S. Caram, Powder Technology **192**, 33 (2009).
[4] J. A. Dijksman, G. H. Wortel, L. T. H. van Dellen, O. Dauchot, and M. van Hecke, Physical Review Letters **107**, 108303 (2011).
[35] A. Pons, T. Darnige, J. Crassous, E. Clément, and A. Amon, EPL (Europhysics Letters) **113**, 28001 (2016).
[36] I. Theurkauff, C. Cottin-Bizonne, J. Palacci, C. Ybert, and L. Bocquet, Physical Review Letters **108**, 268303 (2012).
[37] S. Hilgenfeldt, S. A. Koehler, and H. A. Stone, Physical Review Letters **86**, 4704 (2001).
[38] A. Saint-Jalmes, Soft Matter **2**, 836 (2006).

– Supplementary material –
Non-linear rheology in a model biological tissue

HYBRID STOCHASTIC PROCESS

One underlying interpretation of the Hébraud-Lequeux (HL) model [S1] and its generalisations [S2, S3] is a hybrid stochastic process for the local shear stress $\sigma_i(t)$ and the local yield stress $\sigma_{c,i}(t)$, with i indexing the position of the mesoscopic box on which the local shear is defined. In a simplified mean-field picture, this stochastic process is assumed to be modelled by the following combined Langevin and resetting dynamics:

$$\begin{cases} \partial_t \sigma(t) = G_0 \dot{\gamma} + \xi_{\rm mec}(t) \\ |\sigma| > \sigma_c : \quad \sigma \overset{1/\tau}{\longmapsto} 0 \quad \& \quad \rho(\sigma_c') \end{cases} \tag{S1}$$

with G_0 the average local elastic modulus, and $\dot{\gamma}$ the external shear rate (assumed to be constant). In other words, the local stress $\sigma(t)$ fluctuates diffusively around its external elastic loading $G_0\dot{\gamma}t$, according to a Gaussian noise $\xi_{\rm mec}(t)$ fully determined by:

$$\begin{cases} \langle \xi_{\rm mec}(t) \rangle = 0 \\ \langle \xi_{\rm mec}(t) \xi_{\rm mec}(t') \rangle = 2D(t)\delta(t-t') \end{cases} \tag{S2}$$

Once the local stress $\sigma(t)$ exceeds the local yield stress $\sigma_c(t)$, it might trigger a local plastic event at a fixed plastic rate $1/\tau$, which would in turn fully relax the local stress, and then refresh the local yield stress by picking a random value according to the *a priori* distribution $\rho(\sigma_c')$. The elastic redistribution of stress to the neighbouring sites is taken into account via a coupling of the amplitude $\propto \sqrt{D(t)}$ of the mechanical noise $\xi_{\rm mec}(t)$ to the global plastic activity $\Gamma(t) = \left\langle \frac{1}{\tau}\theta(|\sigma| - \sigma_c) \right\rangle$.

The novelty here is that we allow for two distinct contributions to the mechanical noise, on the one hand $\xi_{\rm pl}(t)$ which stems from the sum of simultaneous plastic events throughout the system, and on the other hand $\xi_{\rm act}(t)$ which stems for instance from the internal activity, as apoptosis and cell division in a biological tissue, or from an external shaking of the system, as in experiments on dense granular materials [S4]. Assuming that both those noises are Gaussian, that they are independent translates, and that we can neglect the correlation in time (*i.e.* that the plastic events are almost simultaneous):

$$\xi_{\rm mec}(t) = \xi_{\rm pl}(t) + \xi_{\rm act}(t), \quad \langle \xi_{\rm pl}(t)\xi_{\rm act}(t) \rangle = 0 \tag{S3}$$

$$\begin{cases} \langle \xi_{\rm pl}(t) \rangle = 0 \\ \langle \xi_{\rm pl}(t) \xi_{\rm pl}(t') \rangle = 2\alpha\Gamma(t)\delta(t-t') \end{cases} \tag{S4}$$

$$\begin{cases} \langle \xi_{\rm act}(t) \rangle = 0 \\ \langle \xi_{\rm act}(t) \xi_{\rm act}(t') \rangle = 2D_0\delta(t-t') \end{cases} \tag{S5}$$

encoding the coupling between the mechanical noise and the plastic activity in the following closure relation:

$$D(t) = \alpha\,\Gamma(t) + D_0 \tag{S6}$$

and the following evolution equation for the probability distribution (PDF) of local stress σ and local yield stress σ_c at a time t:

$$\begin{aligned} \partial_t \mathcal{P}(\sigma, \sigma_c, t) = &- G_0\dot{\gamma}\,\partial_\sigma \mathcal{P} + D(t)\,\partial_\sigma^2 \mathcal{P} \\ &- \frac{1}{\tau}\theta(|\sigma| - \sigma_c)\,\mathcal{P} + \Gamma(t)\,\rho(\sigma_c)\,\delta(\sigma) \end{aligned} \tag{S7}$$

$$\Gamma(t) = \frac{1}{\tau}\int_0^\infty d\sigma_c \int_{|\sigma|>\sigma_c} d\sigma\,\mathcal{P}(\sigma, \sigma_c, t) \tag{S8}$$

The steady state at constant shear rate and $D_0 = 0$ has been studied in Ref. [S2] for a generic distribution $\rho(\sigma_c)$, and previously with respect to the original HL model. Its generalisations with a partial relaxation of stress after a local plastic event are discussed for instance in Ref. [S3], in the broader framework of athermal local-yield stress (ALYS) models.

STEADY-STATE SOLUTION AT FIXED $\dot{\gamma}$

We consider the steady-state solution of the original HL model, adapting the expressions for the disordered HL model given in Ref. [S2] by assuming a single value for the local yield stress σ_c (*i.e.* $\rho(\sigma_c') = \delta(\sigma_c' - \sigma_c)$).

At fixed diffusion coefficient D

We first recall the expressions at fixed diffusion coefficient D for the global plastic activity $\Gamma = \Gamma(D, \dot{\gamma})$ and the mean stress $\sigma_M = \sigma_M(D, \dot{\gamma})$:

$$\Gamma\tau = \frac{D\tau}{\tilde{f}_{\sigma_c}\left(\sqrt{D\tau}, \frac{G_0\dot{\gamma}\tau}{D\tau}\right)} \tag{S9}$$

where the structure of the explicit dependence suggests to define the following variables with $x = \sqrt{D\tau}$ and $y = G_0\dot{\gamma}\tau/x^2$, and

$$\begin{aligned} &\tilde{f}_{\sigma_c}(x, y) - x^2 \\ &= \frac{\sigma_c}{y}\,\frac{1 + \left(\sqrt{1 + \frac{4}{x^2y^2}} + \frac{2}{\sigma_c y}\right)\tanh\left(\frac{\sigma_c y}{2}\right)}{\tanh\left(\frac{\sigma_c y}{2}\right) + \sqrt{1 + \frac{4}{x^2y^2}}} \end{aligned} \tag{S10}$$

These last two equations correspond respectively to Eqs. (10) and (14) of Ref. [S2].

As for the mean stress, we distinguish the contributions of the overstressed sites ($|\sigma| > \sigma_c$) and of the understressed sites ($|\sigma| < \sigma_c$), adapting Eqs. (C7), (C8) and (C9) of Ref. [S2] at fixed σ_c:

$$\sigma_M^{(\text{over})} = G_0\dot{\gamma}\tau \tag{S11}$$

$$\sigma_M^{(\text{under})} = \frac{1}{y}\left[\frac{\sigma_c^2/2 - \tilde{f}_{\sigma_c}(x,y) + x^2}{\tilde{f}_{\sigma_c}(x,y)}\right] + \frac{1}{y^2\,\tilde{f}_{\sigma_c}(x,y)}\frac{2\sigma_c}{\sqrt{1+\frac{4}{x^2y^2}} + \tanh\left(\frac{\sigma_c y}{2}\right)} \tag{S12}$$

$$\sigma_M = \sigma_M^{(\text{over})} + \sigma_M^{(\text{under})} \tag{S13}$$

Together, the last four expressions allow to compute the mean stress as a function of the following parameters $\{G_0, \dot{\gamma}, \tau, \sigma_c, D\}$, or more precisely $\{G_0\dot{\gamma}\tau, \sigma_c, \sqrt{D\tau}\}$.

Solving the modified closure relation at $D_0 > 0$

The non-linear physics in the HL predicted flow curve arises because of the coupling between the plastic activity and the fluctuations of local stress, quantified by the diffusion coefficient. In the original HL model, this coupling was assumed to be linear; here we assume more generally that it is affine with a finite diffusion coefficient threshold $D_0 > 0$. In other words, we start from the closure relation:

$$D = \alpha\,\Gamma(D) + D_0 \tag{S14}$$

$$\iff \alpha\frac{D}{D-D_0} \overset{(\text{S10})}{=} \tilde{f}_{\sigma_c}\left(\sqrt{D\tau}, \frac{G_0\dot{\gamma}\tau}{D\tau}\right) \tag{S15}$$

This equation has unfortunately no explicit analytical solution that would yield $D = D(G_0\dot{\gamma}\tau, \sigma_c, \alpha, \sqrt{D_0\tau})$. Nevertheless, the diffusion coefficient can be geometrically determined by the intersection of $\tilde{f}_{\sigma_c}\left(\sqrt{D\tau}, \frac{G_0\dot{\gamma}\tau}{D\tau}\right)$ and the hyperbola $\frac{\alpha D}{D-D_0}$, as illustrated in Fig. S1. So that $D = D(G_0\dot{\gamma}\tau, \sigma_c, \alpha, \sqrt{D_0\tau})$ can be computed numerically for any given set of its parameters values, using for instance a straightforward bisection method.

The corresponding mean stress can then be obtained by substituting $D = D(G_0\dot{\gamma}\tau, \sigma_c, \alpha, \sqrt{D_0\tau})$ into (S11)-(S12)-(S13), yielding $\sigma_M = \sigma_M(G_0\dot{\gamma}\tau, \sigma_c, \alpha, \sqrt{D_0\tau})$. They are illustrated by Fig. S2.

Low-shear-rate perturbative expansions

In the low-shear-rate regime we are interested in, the previous expressions can be simplified within a perturbative expansion. We are focusing exclusively on the

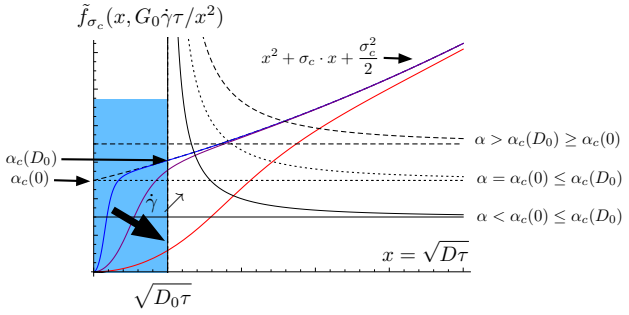

FIG. S1. Schematic plot of the function $\tilde{f}_{\sigma_c}\left(\sqrt{D\tau}, \frac{G_0\dot{\gamma}\tau}{D\tau}\right)$ defined in Eq. (S9), in the presence of a constant external shear rate $\dot{\gamma} \geq 0$. This function in absence of shear, *i.e.* $\tilde{f}_{\sigma_c}\left(\sqrt{D\tau}, 0\right)$, defines the 'critical' coupling $\alpha(0) = \sigma_c^2/2$ of the original HL model, and its counterpart $\alpha(D_0) = \tilde{f}_{\sigma_c}\left(\sqrt{D_0\tau}, 0\right)$ for a finite activity. The steady-state diffusion coefficient is determined geometrically as the α-dependent intersection of $\tilde{f}_{\sigma_c}$ with the hyperbola $\alpha x^2/(x^2 - D_0\tau)$, as illustrated for three different values of α.

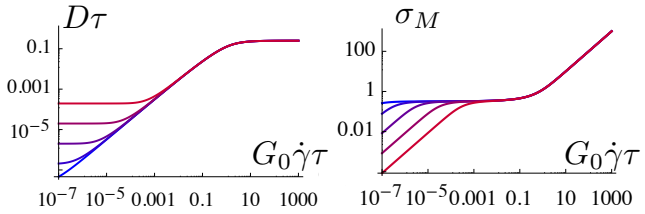

FIG. S2. Steady-state diffusion coefficient and mean stress predicted by the original HL, with a single value for the local yield stress $\sigma_c = 1$, and a fixed coupling $\alpha/\sigma_c^2 = 0.25$. The curves from blue to red correspond to an increasing value for the diffusion threshol $D_0\tau \in \{10^{-8}, 10^{-7}, 10^{-6}, 10^{-5}, 10^{-4}\}$.

regimes at $\alpha < \alpha_c = \sigma_c^2/2$, which displays a Herschel-Bulkley behavior of the flow curve at low shear rates. In addition, we assume that D_0 is sufficiently small so that it is relevant only for shear rates below $\dot{\gamma}_*(D_0)$, with $G_0\dot{\gamma}_*\tau \ll 1$. This assumption allows us on the one hand to assume that the usual HL predictions remain valid for $\dot{\gamma} > \dot{\gamma}_*$, and on the other hand to use the same low-shear-rate perturbative expansion at $\dot{\gamma} < \dot{\gamma}_*$ with $D \approx D_0$.

These two regimes are transparent on the diffusion coefficient itself, at $G_0\dot{\gamma}\tau \ll 1$:

$$\begin{cases} D \approx D_0 & (\text{at } \dot{\gamma} < \dot{\gamma}_*) \\ D \approx C_1 G_0\dot{\gamma}\tau\left[1 + C_2\,(G_0\dot{\gamma}\tau)^{1/2}\right] & (\text{at } \dot{\gamma} > \dot{\gamma}_*) \end{cases} \tag{S16}$$

with C_1 and C_2 given by:

$$\begin{cases} C_1\sigma_c\tanh\left(\frac{\sigma_c}{2C_1}\right) = \alpha \\ C_2 = \sqrt{C_1}\,\frac{\frac{\sigma_c}{2} + C_1\tanh\left(\frac{\sigma_c}{2C_1}\right) - \frac{1}{2}\sigma_c\tanh^2\left(\frac{\sigma_c}{2C_1}\right)}{\frac{\sigma_c^2}{2} - C_1\sigma_c\tanh\left(\frac{\sigma_c}{2C_1}\right) - \frac{1}{2}\sigma_c^2\tanh^2\left(\frac{\sigma_c}{2C_1}\right)} \end{cases} \tag{S17}$$

(see Eqs. (D.10) and (D.11) in Ref. [S2]). The crossover $\dot{\gamma}_*$ can then be simply defined as the intersection of the plateau at D_0 and the linear regime as follows:

$$D_0\tau \equiv C_1 G_0 \dot{\gamma}_*^{(\mathrm{diff})}\tau \Longleftrightarrow \boxed{\dot{\gamma}_*^{(\mathrm{diff})} = \frac{D_0}{G_0 C_1} \sim D_0} \quad \text{(S18)}$$

The different features of the diffusion-coefficient regimes are thus characterized by $\left\{D_0, C_1, C_2, \dot{\gamma}_*^{(\mathrm{diff})}\right\}$.

The mean stress also has two regimes as a function of the shear rate at $G_0\dot{\gamma}\tau \ll 1$, consequently to (S16):

$$\begin{cases} \sigma_M \approx \tilde{\eta}\, G_0\dot{\gamma}\tau = \eta\,\dot{\gamma} & (\text{at } \dot{\gamma} < \dot{\gamma}_*) \\ \sigma_M \approx \sigma_Y + A\,(G_0\dot{\gamma}\tau)^{1/2} = \sigma_y + A_{\mathrm{HB}}\,\dot{\gamma}^{1/2} & (\text{at } \dot{\gamma} > \dot{\gamma}_*) \end{cases} \quad \text{(S19)}$$

where we have introduced two different notations for the parameters, depending if they include $G_0\tau$ or not. The explicit expressions for the Herschel-Bulkley behavior at $\dot{\gamma} > \dot{\gamma}_*$ are the following:

$$\sigma_Y = C_1 \left[\frac{\sigma_c^2/2}{C_1\sigma_c \tanh\left(\frac{\sigma_c}{2C_1}\right)} - 1 \right] \quad \text{(S20)}$$

$$A = \frac{A_{\mathrm{HB}}}{G_0\tau} = \frac{3\sqrt{C_1}}{2}\coth\left(\frac{\sigma_c}{2C_1}\right) + \frac{C_1^{3/2}}{\sigma_c}\left(1 + \frac{\cosh\left(\frac{\sigma_c}{C_1}\right) - 1}{1 - \frac{C_1}{\sigma_c}\sinh\left(\frac{\sigma_c}{C_1}\right)}\right) \quad \text{(S21)}$$

(recalled from Eqs. (19)-(20) of Ref. [S2], and detailed furthermore in Appendix E of the same reference). Note that keeping track of the second order correction C_2 is necessary in order to obtain the correct expression for A. As for the Newtonian behaviour at $\dot{\gamma} > \dot{\gamma}_*$, its viscosity is given by:

$$\begin{aligned} \tilde{\eta} = \frac{\eta}{G_0\tau} &= 1 + \left(\frac{\sigma_c^3}{6\sqrt{D_0\tau}} + \frac{\sigma_c^4}{24 D_0\tau}\right)\frac{1}{\tilde{f}_{\sigma_c}\left(\sqrt{D_0\tau}, 0\right)} \\ &= 1 + \left(\frac{\sigma_c^3}{6\sqrt{D_0\tau}} + \frac{\sigma_c^4}{24 D_0\tau}\right)\frac{1}{D_0\tau + \sqrt{D_0\tau}\sigma_c + \sigma_c^2/2} \end{aligned} \quad \text{(S22)}$$

The crossover $\dot{\gamma}_*$ can then be defined similarly to (S18) as the intersection of the plateau at the Newtonian regime $\eta\,\dot{\gamma}$ and the yield-stress plateau σ_Y as follows:

$$\eta\dot{\gamma}_*^{(\mathrm{stress})} \equiv \sigma_Y \Longleftrightarrow \boxed{\dot{\gamma}_*^{(\mathrm{stress})} = \frac{\sigma_Y}{\eta} = \frac{\sigma_Y}{\tilde{\eta} G_0\tau}} \quad \text{(S23)}$$

The dependence on the threshold D_0 is hidden in the viscosity $\tilde{\eta}$, which can be perturbatively expanded at small D_0 as:

$$\tilde{\eta} \underset{(D_0\to 0)}{\approx} \frac{\sigma_c^2}{12 D_0\tau} + \frac{\sigma_c}{6\sqrt{D_0\tau}} + \frac{1}{2} + \mathcal{O}(\sqrt{D_0\tau}) \quad \text{(S24)}$$

So we recover that $\dot{\gamma}_*^{(\mathrm{stress})} \sim D_0$, as in (S18), although this scaling prefactor differs depending on the criterion used to define the crossover $\dot{\gamma}_*$, either on the diffusion coefficient or on the mean-stress crossover. The different features of the mean-stress regimes are thus characterized by $\left\{\eta, \sigma_Y, A_{\mathrm{HB}}, \dot{\gamma}_*^{(\mathrm{stress})}\right\}$.

The equation for $C_1(\sigma_c, \alpha)$ being implicit, the crossover expression can be further simplified only in two specific opposite cases for $\alpha < \alpha_c$, for both our definitions of $\dot{\gamma}_*(D_0)$. One the one hand:

$$\begin{cases} G_0\dot{\gamma}_*^{(\mathrm{diff})} \approx D_0\sigma_c/\alpha & (\text{at } \alpha \ll \alpha_c) \\ G_0\dot{\gamma}_*^{(\mathrm{diff})} \approx D_0\left[24(\alpha_c - \alpha)\right]^{1/2}/\sigma_c^2 & (\text{at } \alpha \lesssim \alpha_c) \end{cases} \quad \text{(S25)}$$

and on the other hand:

$$\dot{\gamma}_*^{(\mathrm{stress})} = \frac{\sigma_Y}{\tilde{\eta} G_0\tau} = \frac{12\sigma_Y D_0}{\sigma_c^2 G_0} \quad \text{(S26)}$$

$$\begin{cases} G_0\dot{\gamma}_*^{(\mathrm{stress})} \sim D_0\frac{\alpha_c - \alpha}{\sigma_c^3} & (\text{at } \alpha \ll \alpha_c) \\ G_0\dot{\gamma}_*^{(\mathrm{stress})} \sim D_0\frac{(\alpha_c - \alpha)^{1/2}}{\sigma_c^2} & (\text{at } \alpha \lesssim \alpha_c) \end{cases} \quad \text{(S27)}$$

using the perturbative expansions given in Eqs. (D.13), (D.14), (E.3) and (E.4) in Ref. [S2].

The different features that we have just discussed corresponds to low-shear-rate expansions of the analytical steady-state solution of the model, and can be summarized as follows:

$$\begin{cases} D = D(G_0\dot{\gamma}\tau, \sigma_c, \alpha, \sqrt{D_0\tau}) \\ \text{and features to fit are } \left\{D_0, C_1, C_2, \dot{\gamma}_*^{(\mathrm{diff})}\right\} \end{cases} \quad \text{(S28)}$$

$$\begin{cases} \sigma_M = \sigma_M(G_0\dot{\gamma}\tau, \sigma_c, \alpha, \sqrt{D_0\tau}) \\ \text{and features to fit are } \left\{\eta, \sigma_Y, A_{\mathrm{HB}}, \dot{\gamma}_*^{(\mathrm{stress})}\right\} \end{cases} \quad \text{(S29)}$$

The shear-rate dependence of the stress diffusion coefficient $D(\dot{\gamma})$ and the corresponding flow curve $\sigma_M(\dot{\gamma})$ are shown in Fig. S2.

We mention at last that the validity of these mean-field predictions is discussed, at a qualitative level, in the broader framework of the athermal local-yield stress (ALYS) models at fixed shear rate, in Ref. [S3]. We know in particular that the Herschel-Bulkley behaviour of exponent 1/2 is robust with respect to a partial relaxation of stress, although the specific predictions for $\{\sigma_Y, A_{\mathrm{HB}} = A\,G_0\tau\}$ will depend on the *a priori* distribution $\rho(\sigma_c)$, and on the specific partial relaxation of the local stress after a plastic event. The prediction for a Newtonian regime $\sigma_M \approx \eta(D_0)\,\dot{\gamma}$ at very low shear rates is similarly robust to the addition of disorder and partial relaxation. This means in particular that the collapse of the flow curves using that $\dot{\gamma}_* \sim D_0$ should remain valid.

FURTHER MODEL DETAILS AND GPU-PARALLEL MOLECULAR DYNAMICS IMPLEMENTATION

A remarkable amount of information about collective behavior at tissue level can be obtained from effective models where cells are treated as soft elastic objects. Particle-based tissue models have been successfully applied to a wide range of systems, for a complete review see Drasdo *et al.* [S5] and references therein. Here we follow a similar approach and consider a model where the cells are represented by soft spheres of radius b_i. Therefore, the tissue consists in a collection of N such spheres with radii b_i interacting via a soft elastic potential given by,

$$V_{ij} = \begin{cases} \frac{1}{2} k b_{ij}^2 \left[\left(\frac{r_{ij}}{b_{ij}} - 1 \right)^2 - \epsilon^2 \right] & \text{if } \frac{r_{ij}}{b_{ij}} - 1 \leq \epsilon \\ -\frac{1}{2} k b_{ij}^2 \left(\frac{r_{ij}}{b_{ij}} - 1 - 2\epsilon \right)^2 & \text{if } \epsilon < \frac{r_{ij}}{b_{ij}} - 1 \leq 2\epsilon, \end{cases} \tag{S30}$$

where k is the stiffness constant, $b_{ij} = b_i + b_j$ is the sum of the particle radii, and $(b_{ij}\epsilon)$ is the adhesive force strength. The corresponding force of Eq. (S30) is given by Eq. (1) in the main text (see Fig. S3).

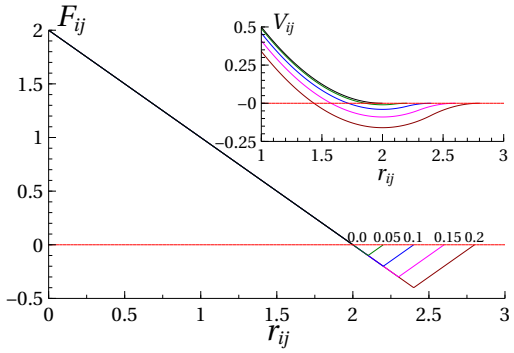

FIG. S3. The elastic force [Eq. (1) in the main text] for $k = 1$ and different values of the adhesive force strength ϵ, as indicated in the figure. (*Inset*) Interparticle potential V_{ij}, given in Eq. (S30).

Neglecting inertia effects we model the dynamics of the cell positions $\mathbf{r}_i(t)$ as fully overdamped [S6]

$$\partial_t \mathbf{r}_i(t) = \mu \mathbf{F}_i, \tag{S31}$$

where μ is the inverse friction coefficient and $\mathbf{F}_i = \sum_{j \neq i} \mathbf{F}_{ij}$ is the total force acting on particle i exerted by its neighbours. We integrate the equation of motion (S31) using a C++ GPU-parallel Molecular Dynamics code described in the following section.

GPU-Parallel Implementation

It is well known that Molecular Dynamics (MD) simulation is a highly parallelizable numerical method. Following the spirit of MD packages such as LAMMPS, AMBER, GROMACS, etc., we have built our own parallel MD code on GPU (NVIDIA CUDA). In contrast to LAMMPS, for example, our in-house code is specifically designed to introduce different sources of activity into the system (cell division, cell death and self-propulsion velocities). The general workflow of the code is shown in algorithm 1. All our routines are fully implemented on the GPU, so that there are no transfers between DEVICE-HOST during the MD execution. The only routines executed by the host (colored in blue) are those required by the user in order to save data. It is worth mentioning that these operations require data transfer between the DEVICE and the HOST, see the red colored text.

Our CUDA kernels are moderately optimized, trying to keep aligned and coalesced memory access, and avoiding threads divergence and atomic functions. Further optimizations are still possible, but there are diminishing returns since at some point they will obfuscate the code for a negligible speedup. As defensive programming techniques we use assertions, and each routine is independently tested before implementation. We do not use heavy database implementations and/or post-processing packages: in most cases the output of our simulation is already the final result. Finally, we used external imaging routines for visualization, testing and presentation purposes.

Algorithm 1: Typical Simulation Scheme

(0) Give atoms initial positions and velocities;
for *Simulation time* **do**
(1) Predict next atom positions:
(a) Get Forces;
(b) Move Atoms and Update Velocities;
(c) Apply Boundary Conditions;
(c*) Deform the box during force-shear simulations;
(2) Cell Functions:
(a) Cell death;
(b) Cell division;
(3) Build neighbours:
if ***(2)*** *or atoms move too far* **then**
(a) Build the linked-list;
(b) Using (a) build the neighbour list of each atom;
(4) Analysis:
if *Simulation time* **then**
(a) Standard properties: pressure, density, etc.;
(b) Transport properties: Mean square displacement etc.;
(c) Transfer (a) and (b) to the host (CPU);
(d) Save (a) (b);
(5) Save Configurations:
if *Simulation time* **then**
(a) Transfer atom properties to the host (CPU);
(b) Save (a);

* daniel-alejandro.matoz-fernandez@univ-grenoble-alpes.fr

† elisabeth.agoritsas@lpt.ens.fr

[S1] P. Hébraud and F. Lequeux, Phys. Rev. Lett. **81**, 2934 (1998).

[S2] E. Agoritsas, E. Bertin, K. Martens, and J.-L. Barrat, Eur. Phys. J. E **38**, 71 (2015).

[S3] E. Agoritsas and K. Martens, "Nontrivial rheological exponents in sheared yield stress fluids," arXiv:1602.03484 [cond-mat.soft] (2016).

[S4] J. A. Dijksman, G. H. Wortel, L. T. H. van Dellen, O. Dauchot, and M. van Hecke, Phys. Rev. Lett. **107**, 108303 (2011).

[S5] D. Drasdo, S. Hoehme, and M. Block, J. Stat. Phys. **128**, 287 (2007).

[S6] S. Henkes, Y. Fily, and M. C. Marchetti, Phys. Rev. E **84**, 84 (2011).